Supporting Information

In-situ confined growth of ultrasmall perovskite quantum dots in metal-organic frameworks and their quantum confinement effect

Ziren Xie,[abc] Xingjun Li,*[ac] Renfu Li,[a] Shan Lu,[ac] Wei Zheng,[ac] Datao Tu,[ac] Yanhui Feng[a] and Xueyuan Chen*[abcd]

[a]*CAS Key Laboratory of Design and Assembly of Functional Nanostructures, Fujian Key Laboratory of Nanomaterials, Fujian Institute of Research on the Structure of Matter, Chinese Academy of Sciences, Fuzhou, Fujian 350002, China.*

[b]*School of Physical Science and Technology, ShanghaiTech University, Shanghai 201210, China.*

[c]*University of Chinese Academy of Sciences, Beijing 100049, China.*

[d]*Fujian Science & Technology Innovation Laboratory for Optoelectronic Information of China, Fuzhou, Fujian 350108, China.*

E-mail: lixj@fjirsm.ac.cn or xchen@fjirsm.ac.cn; Fax: +86 591 63179421; Tel: +86 591 63179421.

Experimental Section

Chemicals and materials: Zirconium tetrachloride ($ZrCl_4$, 99.5%), Terephthalic acid (H_2BDC, 98%) and isopropanol (IPA, analytical reagent) were purchased from Aladdin Chemistry, China. Lead acetate ($Pb(Ac)_2 \cdot 3H_2O$, 99.5%), *N, N*-dimethylformamide (DMF, analytical reagent), ethanol (EtOH, analytical reagent) and benzoic acid (C_6H_5COOH, 99.8%) were purchased from Sinopharm Chemical Reagent Co., China. Methylammonium bromide (MABr, 98.0%) was purchased from TCI (Shanghai) Development Co., Ltd. All chemical reagents were used directly without any further purification. Ultrapure water was used throughout.

Synthesis of UiO-66 Nanoparticles (NPs): The UiO-66 NPs were synthesized by a solvothermal method, basically according to the reported literature.[1] In a typical synthetic process, 0.343 mmol of $ZrCl_4$, 0.343 mmol of H_2BDC and 17 mmol of C_6H_5COOH were first dissolved in a 20 mL of DMF solution, then the mixture was sealed in a 25 mL Teflon-lined stainless steel autoclave and heated at 120 °C for 24 h, followed by cooling down to RT. The obtained UiO-66 nanoparticles were collected by centrifugation, washed with DMF and EtOH several times, and dried at 60 °C in an oven for 12 h.

Synthesis of Pb^{2+}@UiO-66 precursors: The Pb^{2+}@UiO-66 precursors were prepared by immersing the UiO-66 NPs in different concentration (10, 20, 30, 40, 50 and 60 mg/mL) of $Pb(Ac)_2 \cdot 3H_2O$ solutions. Typically, 50 mg UiO-66 NPs were dispersed in 10 mL of $Pb(Ac)_2 \cdot 3H_2O$ ultrapure water solution (10 mg/mL), the mixture was left to stir at 60 °C for 30 min. The Pb^{2+}@UiO-66 precursor with 10 mg/mL of Pb^{2+} ions (denoted as Pb^{2+}@UiO-66-10) was collected by centrifugation and washed with DMF and IPA for several times. Other Pb^{2+}@UiO-66 precursors were synthesized through a similar process by changing the concentration of $Pb(Ac)_2 \cdot 3H_2O$ to the corresponding values.

Synthesis of $MAPbBr_3$@UiO-66 composites: All acquired Pb^{2+}@UiO-66 precursor from the previous step was soaked and stirred in a MABr IPA solution (10 mL, 5 mg/mL) for about 12 h at RT. Then the final $MAPbBr_3$@UiO-66 composites were obtained by centrifugation and washed with IPA for several times. The various $MAPbBr_3$@UiO-66 composites were denoted as $MAPbBr_3$@UiO-66-X (X = 10-60), in which X (in unit of mg/mL) stands for the corresponding Pb^{2+} concentration in the precursors.

Water stability test: 10 mg of $MAPbBr_3$@UiO-66-50 or pure $MAPbBr_3$ samples were immersed in 200 μL of ultrapure water within a well of a 96-well plate. The PL intensity of the samples was recorded by using a microplate reader (SYNERGY H1 HYBRID, BioTeK, USA Production) with an interval of 10 min for 150 min.

Thermal stability test: To investigate the thermal stability of the $MAPbBr_3$@UiO-66 composites, the samples were placed on a thermal stage (77-873 K, THMS 600, Linkam Scientific Instruments) and heated at a temperature range from 298 to 498 K. The PL emission spectra of the samples were recorded by the FLS980 spectrometer upon excitation at 365 nm using a xenon lamp.

Materials characterization:

Powder X-ray diffraction (XRD) patterns of the samples were recorded with an X-ray diffractometer (Miniflex II, Rigaku) with Cu Kα1 radiation (λ = 0.154187 nm). Both the low- and high-resolution transmission electron microscopy (TEM) measurements were performed by using a TECNAI G^2 F20 TEM equipped with an energy dispersive X-ray (EDX) spectrometer. The scanning electron microscopy (SEM) measurements were performed by using a JSM-6700F SEM equipped with the energy dispersive X-ray (EDX) spectroscopy. The chemical composition of the samples was analyzed by inductively coupled plasma-atomic emission spectroscopy (ICP-AES, Ultima2, Jobin Yvon). Fourier transform infrared spectra (FTIR) were recorded on a Magna 750 FTIR spectrometer. Thermogravimetric analysis (TGA) experiments were conducted on a Netzsch STA449C thermal analysis system under N_2 atmosphere at a rate of 10 °C/min. The gas adsorption measurement was performed on an ASAP 2020 Surface Area and Pore Size Analyzer, which was performed at 77 K in a liquid nitrogen bath. The PL excitation and emission spectra were measured using an Edinburgh Instrument FLS980 spectrometer equipped with a 450 W xenon lamp as the excitation sources. The absolute quantum yield (QY) of $MAPbBr_3$@UiO-66 composites was measured at RT by employing a barium sulfate coated integrating sphere (150 mm in diameter, Edinburgh) as the sample chamber that was mounted on the FLS980 spectrometer with the entry and output port of the sphere located in 90º geometry from each other in the plane of the spectrometer. A standard tungsten lamp was used to correct the optical response of the instrument. All the spectral data collected were corrected for the

spectral response of both the spectrometer and the integrating sphere. PL photographs of $MAPbBr_3$@UiO-66 composites were taken by using iPhone 11 without using any filter. For PL decay measurement, the samples were excited by using a 375 nm ps-pulsed laser with a focus spot of about 0.01 cm^2. Each curve was fitted with a biexponential function of the form $I_{PL}(t) = A_1 e^{-\frac{t}{\tau_1}} + A_2 e^{-\frac{t}{\tau_2}}$, and the average decay lifetime was calculated as $< \tau_L >= \frac{A_1\tau_1^2 + A_2\tau_2^2}{A_1\tau_1 + A_2\tau_2}$.

Supplementary Figures and Tables

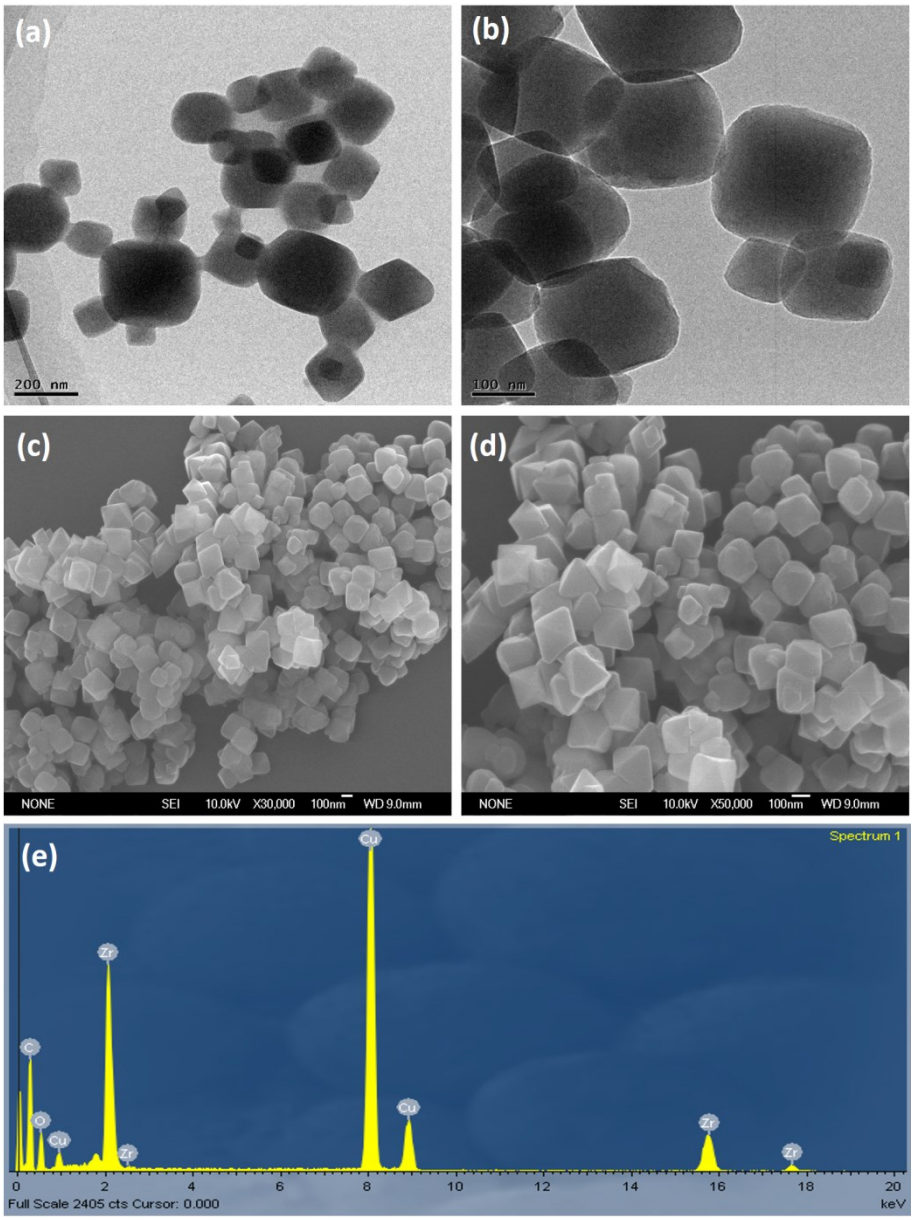

Figure S1. (a, b) TEM images of the UiO-66 NPs. (c, d) SEM images of the UiO-66 NPs. (e) EDX analysis of the UiO-66 NPs which reveals the presence of the elements of Zr, O and C.

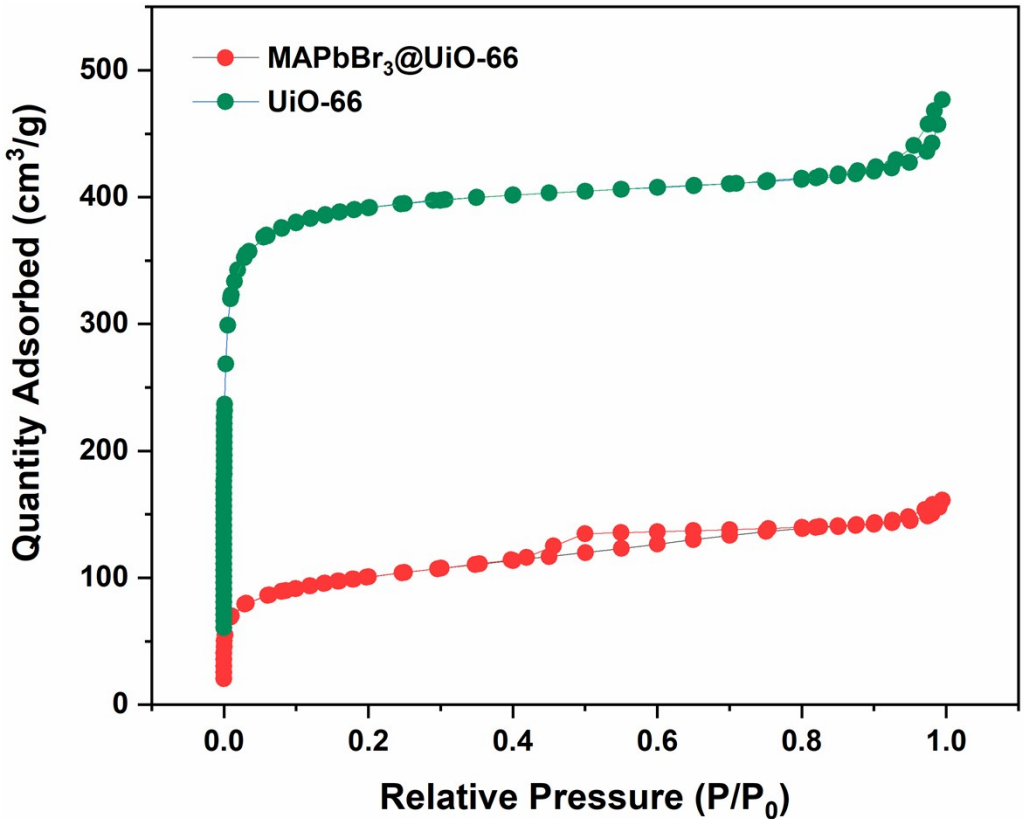

Figure S2. N_2 adsorption isotherms obtained for UiO-66 NPs and $MAPbBr_3$@UiO-66-50 composites at 77 K. The N_2 adsorption isotherm at 77 K showed that UiO-66 NPs and $MAPbBr_3$@UiO-66-50 displayed type-I adsorption behavior with a BET surface area of 1522 m^2g^{-1} and 359 m^2g^{-1}.

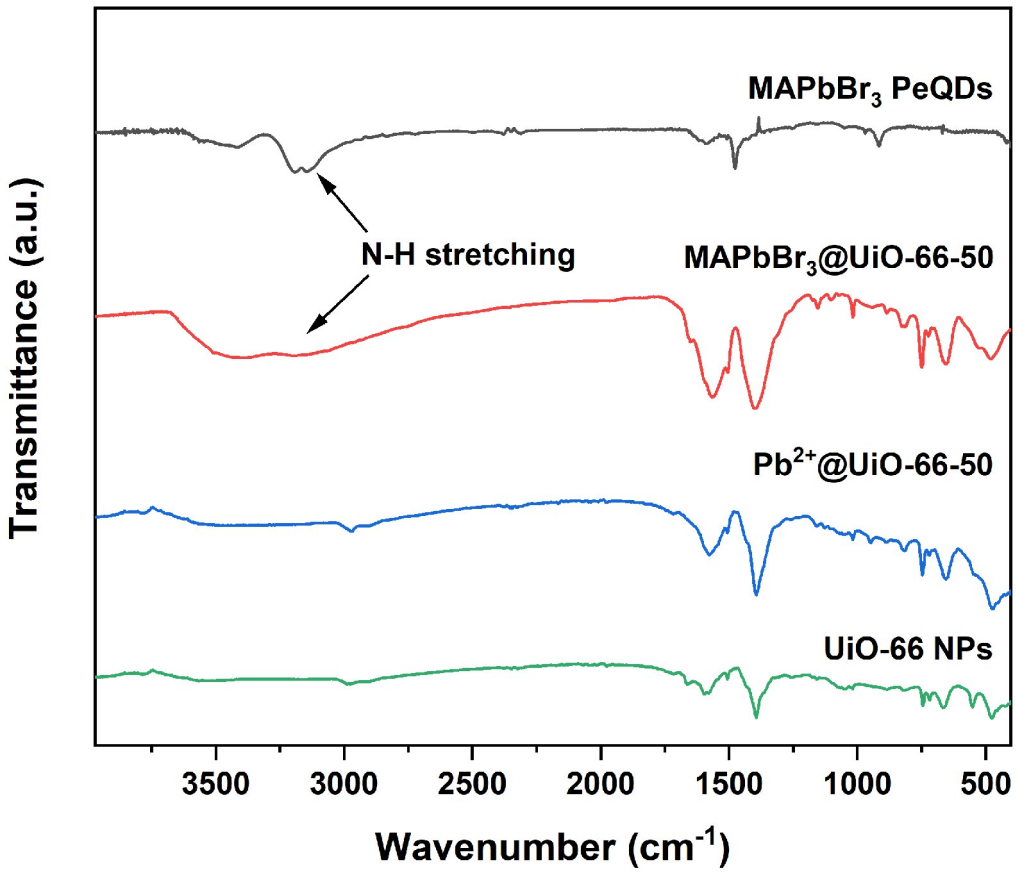

Figure S3. FTIR of the $MAPbBr_3$ PeQDs, UiO-66 NPs, Pb^{2+}@UiO-66-50 precursors and $MAPbBr_3$@UiO-66-50 composites. One intense broad IR band centered at 3180 cm^{-1} was observed in both $MAPbBr_3$ PeQDs and $MAPbBr_3$@UiO-66-50 composites, which was attributed to the stretching vibrations of N-H bands of $CH_3NH_3^+$.

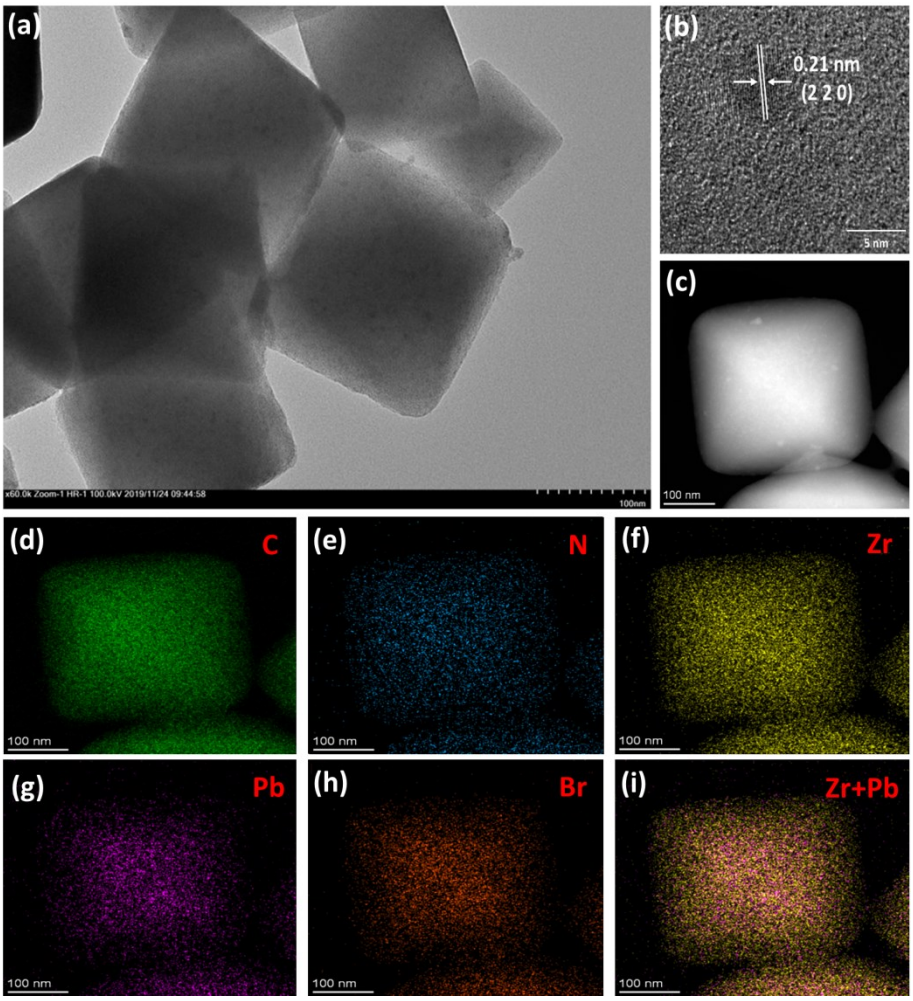

Figure S4. (a) Bright field TEM and (b) HRTEM images of $MAPbBr_3$@UiO-66-10 composites with lattice spacing of $MAPbBr_3$ PeQDs. (c) HAADF-STEM image of $MAPbBr_3$@UiO-66-10 composites. (d-i) Elemental mapping diagrams of $MAPbBr_3$@UiO-66-10 composites.

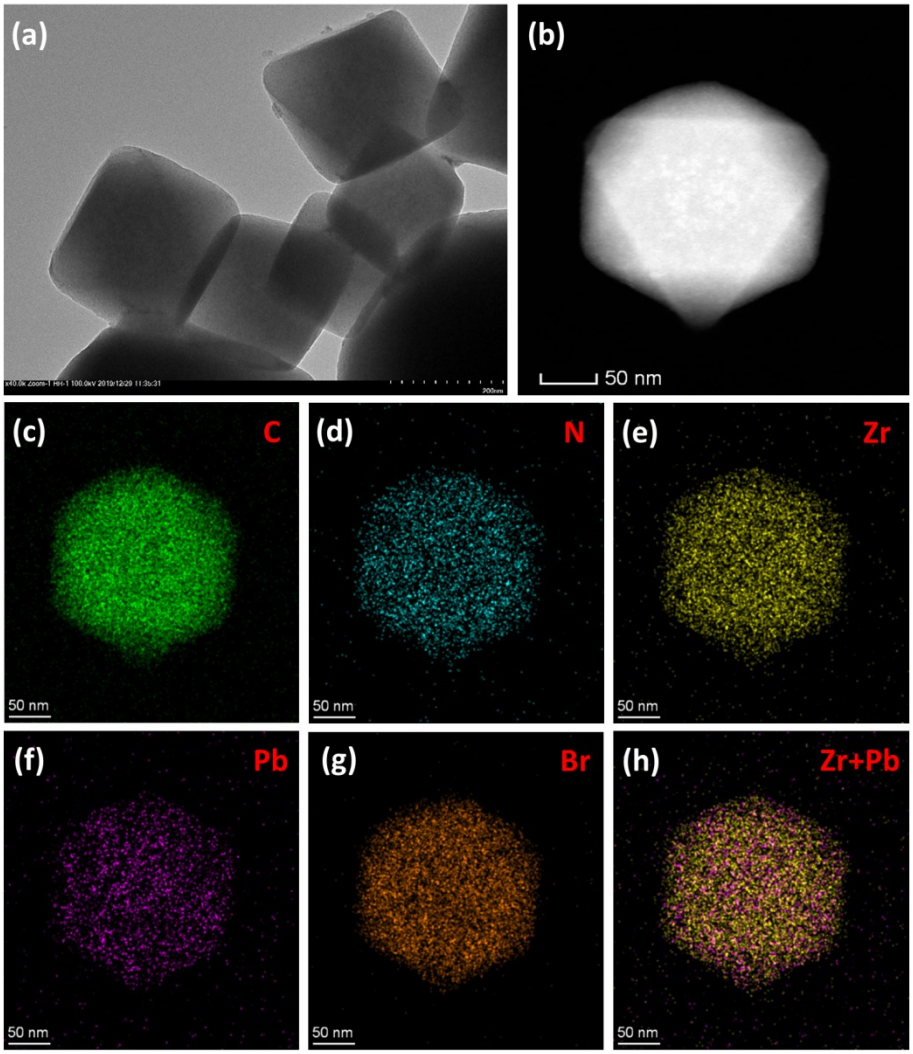

Figure S5. (a) Bright field TEM and (b) HAADF-STEM images of $MAPbBr_3$@UiO-66-20 composites. (c-h) Elemental mapping diagrams of $MAPbBr_3$@UiO-66-20 composites.

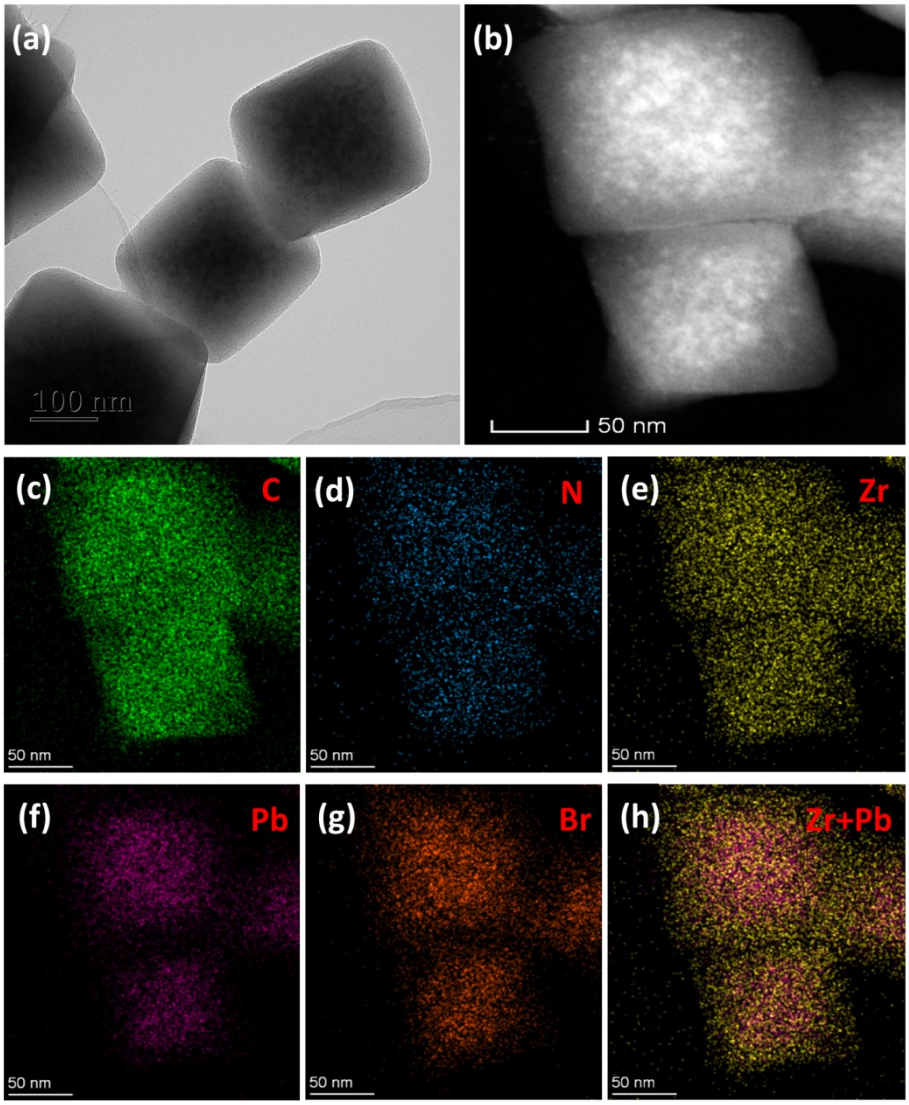

Figure S6. (a) Bright field TEM and (b) HAADF-STEM images of $MAPbBr_3$@UiO-66-30 composites. (c-h) Elemental mapping diagrams of $MAPbBr_3$@UiO-66-30 composites.

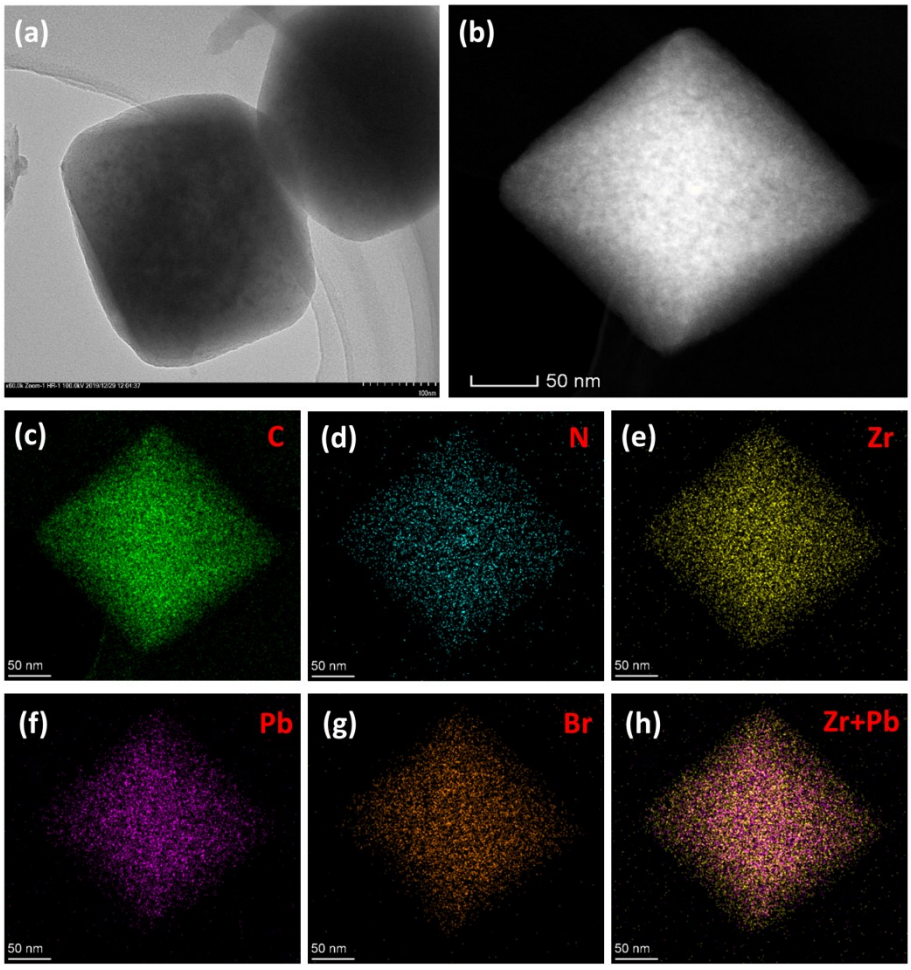

Figure S7. (a) Bright field TEM and (b) HAADF-STEM images of $MAPbBr_3$@UiO-66-40 composites. (c-h) Elemental mapping diagrams of $MAPbBr_3$@UiO-66-40 composites.

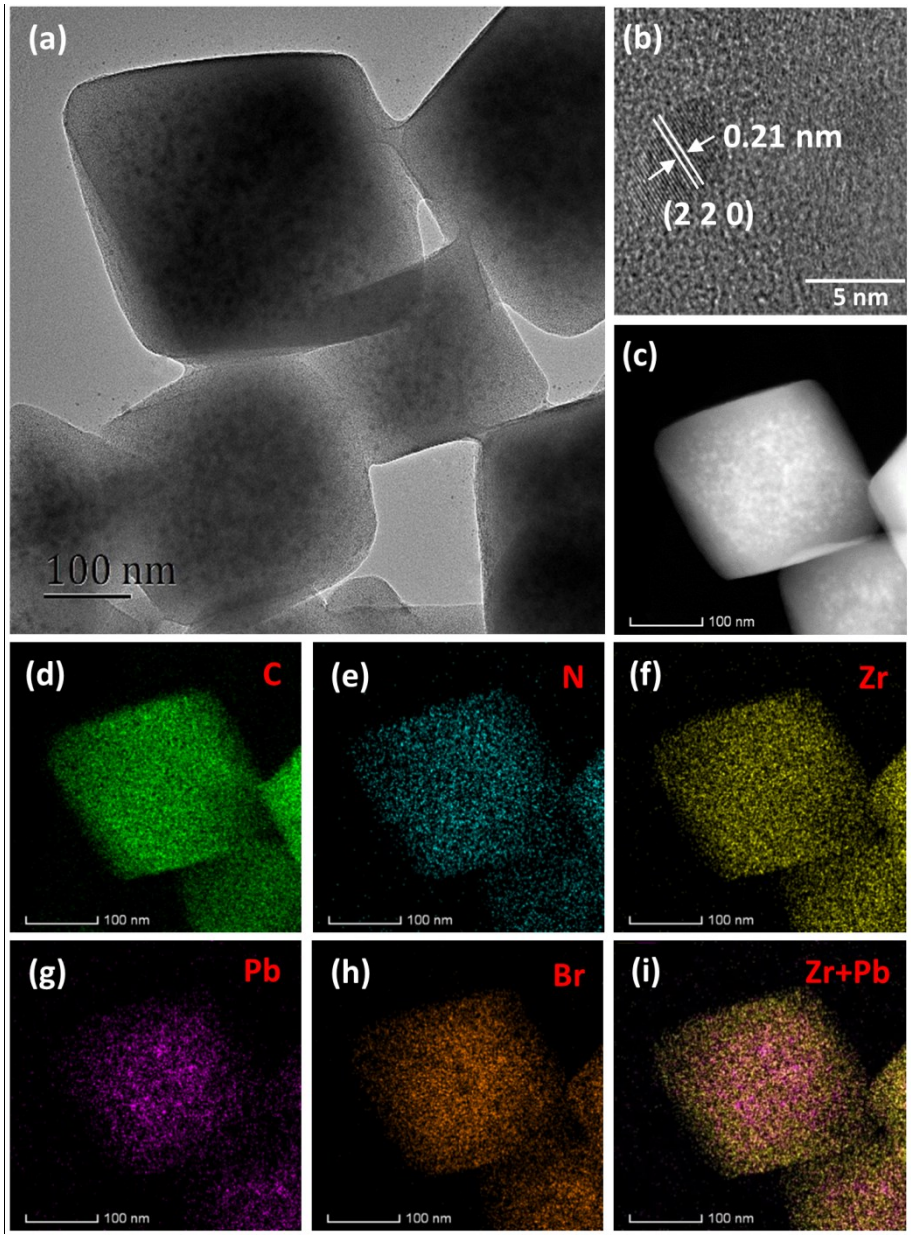

Figure S8. (a) Bright field TEM and (b) HRTEM images of $MAPbBr_3$@UiO-66-50 composites with lattice spacing of $MAPbBr_3$ PeQDs. (c) HAADF-STEM image of $MAPbBr_3$@UiO-66-50 composites. (d-i) Elemental mapping diagrams of $MAPbBr_3$@UiO-66-50 composites.

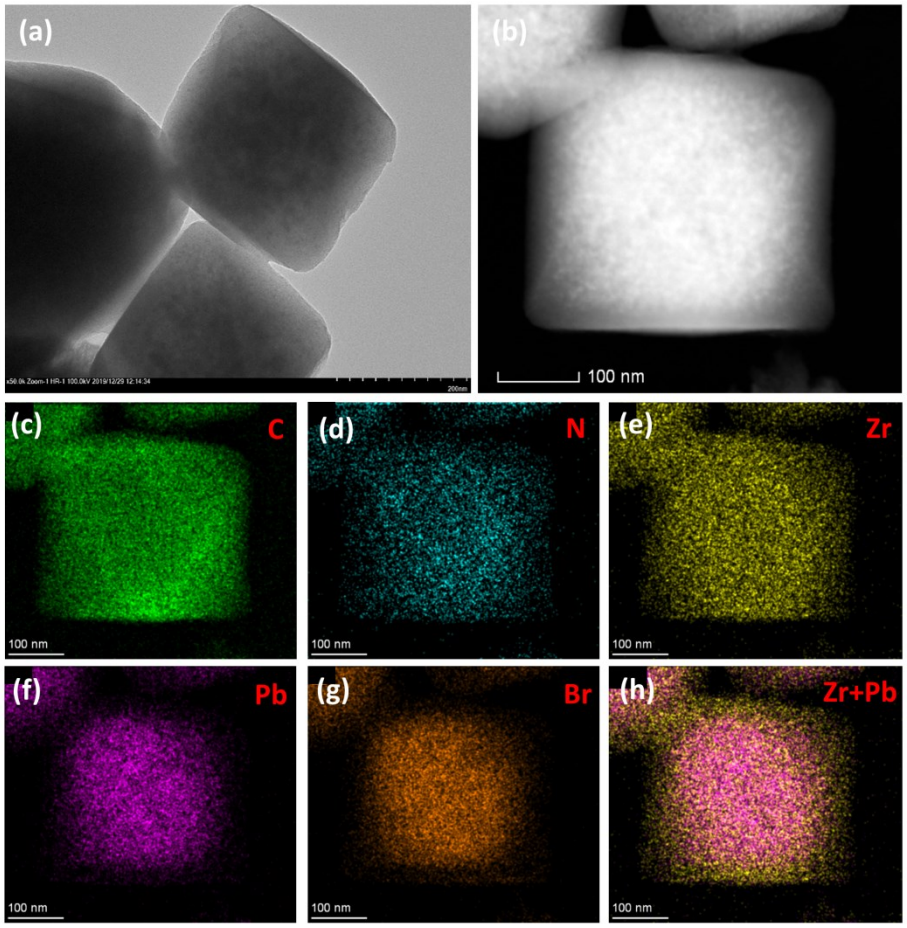

Figure S9. (a) Bright field TEM and (b) HAADF-STEM images of $MAPbBr_3$@UiO-66-60 composites. (c-h) Elemental mapping diagrams of $MAPbBr_3$@UiO-66-60 composites.

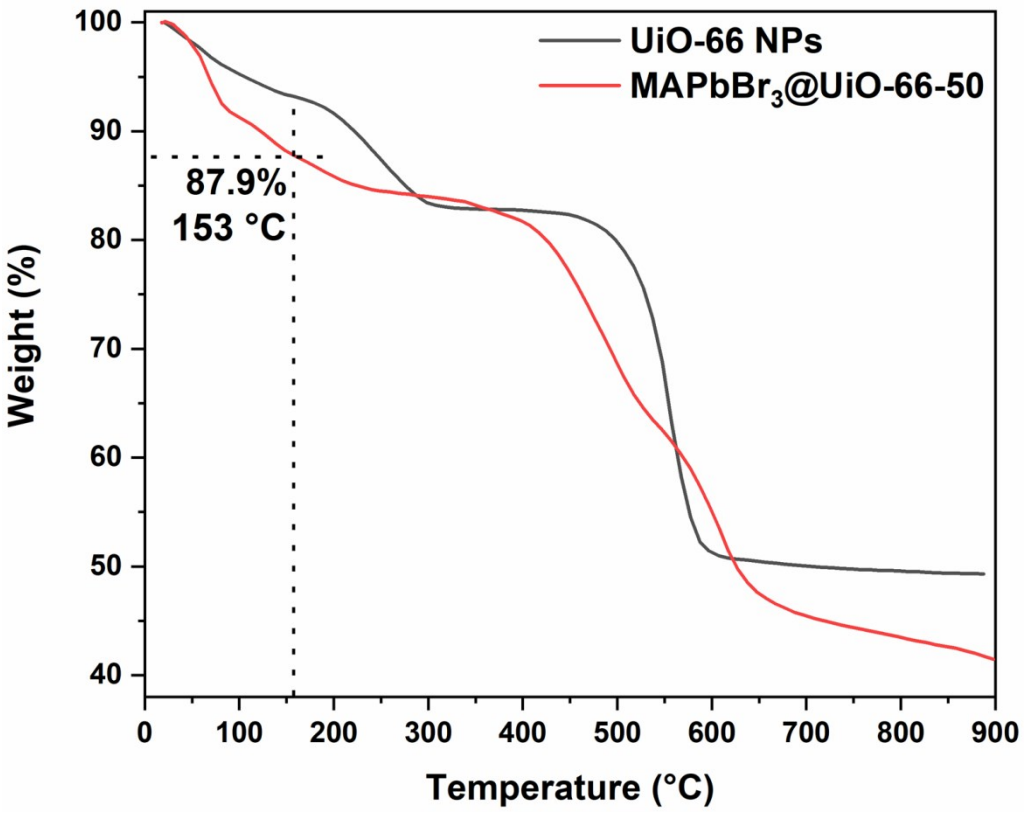

Figure S10. TGA curve of the UiO-66 NPs and $MAPbBr_3$@UiO-66-50 composites obtained by heating them under N_2 atmosphere in the temperature range of 20-900 ^oC at a rate of 10 ^oC/min. The first weight loss of $MAPbBr_3$@UiO-66 (50 mg/mL) of 8.8% was from 20 to 100 ^oC, which corresponds to the loss of the DMF molecules and $MAPbBr_3$ NPs in the interior of the UiO-66 NPs.

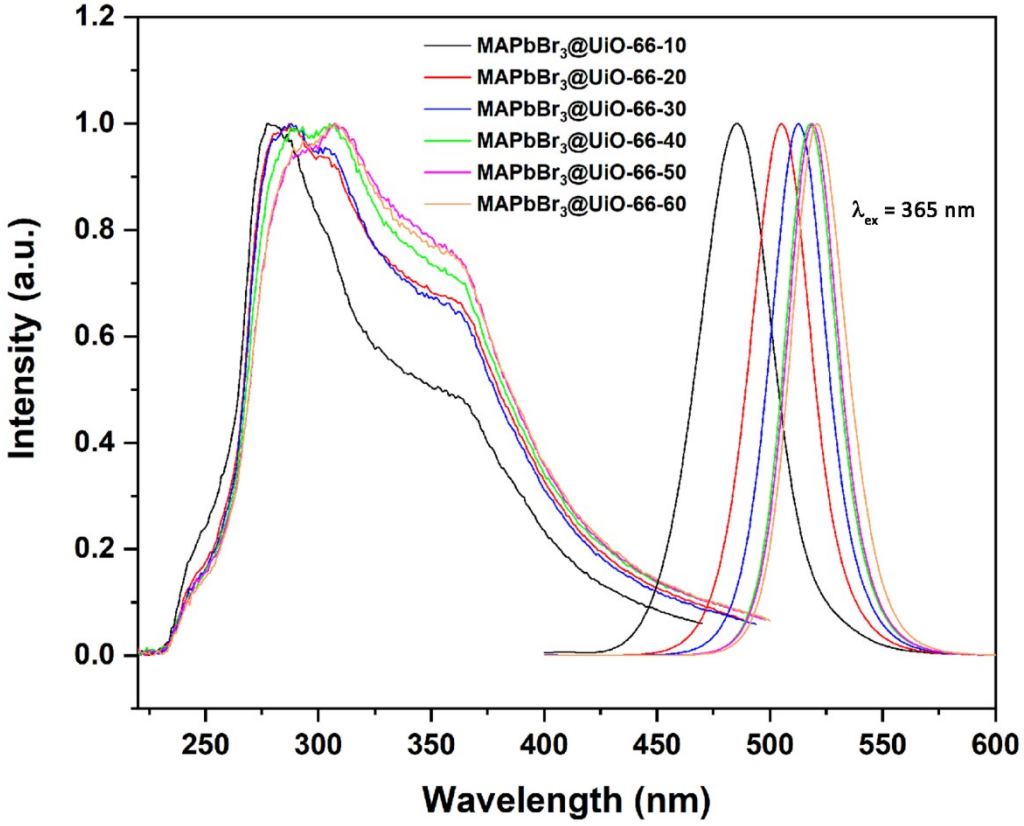

Figure S11. PL excitation spectra (λ_{em} = 486, 505, 514, 518, 519 and 521 nm, respectively) and emission spectra (λ_{ex} = 365 nm) of the $MAPbBr_3$@UiO-66 composites.

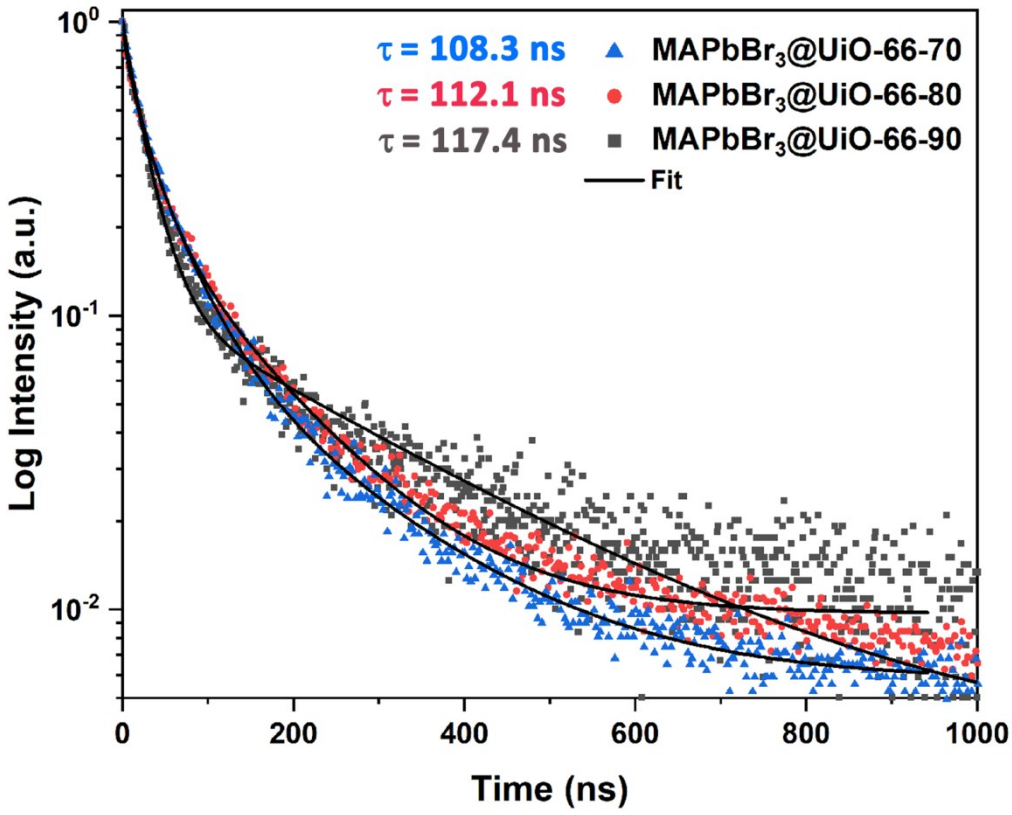

Figure S12. PL decays of the $MAPbBr_3$@UiO-66 composites with Pb^{2+} concentrations of 70-90 mg/mL.

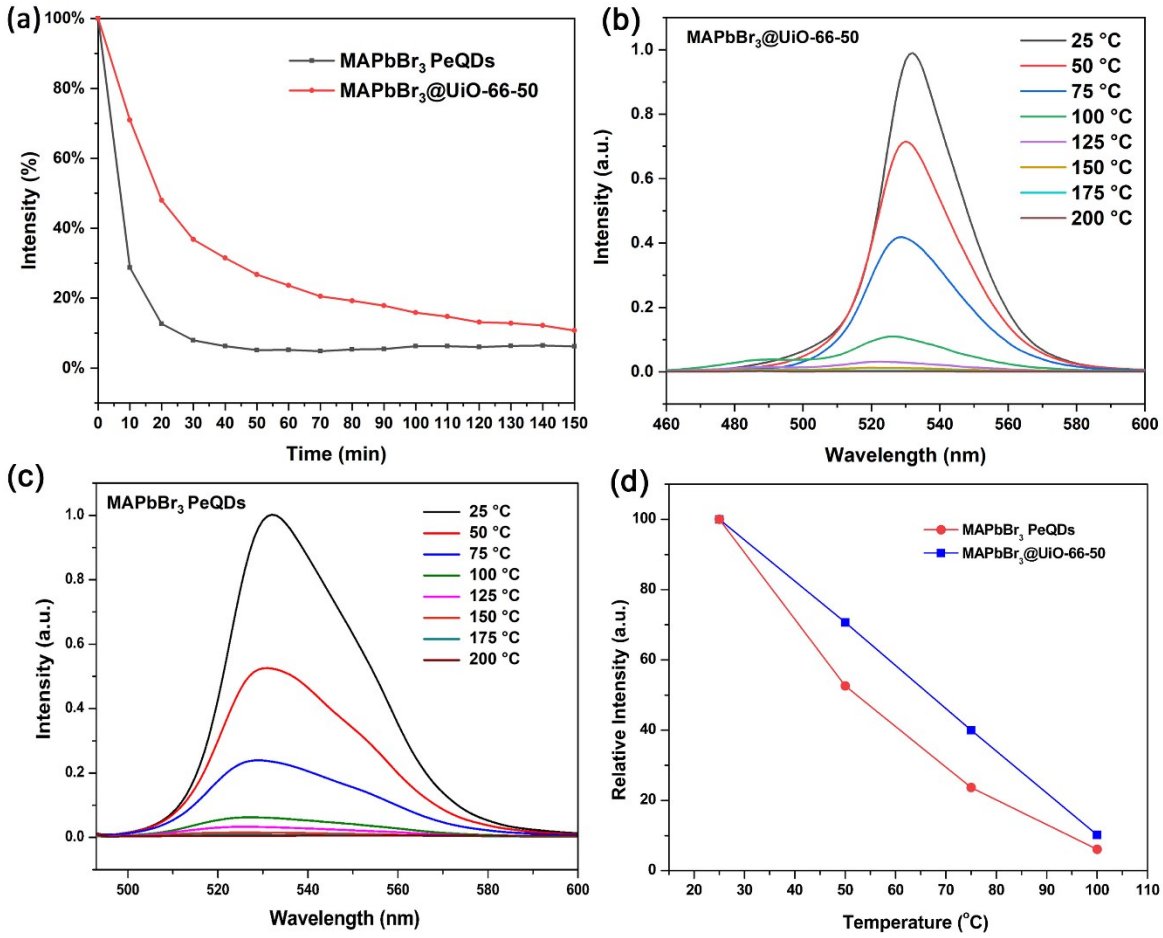

Figure S13. Water and Thermal stability investigations of $MAPbBr_3$@UiO-66 composites: (a) PL emission intensities of pure $MAPbBr_3$ PeQDs and $MAPbBr_3$@UiO-66 composites immersed in water at different times. (b) Temperature-dependent PL emission spectra of $MAPbBr_3$@UiO-66-50 composites and (c) pure $MAPbBr_3$ PeQDs upon excitation at 365 nm. (d) A comparison of relativity PL intensities of $MAPbBr_3$@UiO-66-50 composites and pure $MAPbBr_3$ PeQDs upon excitation at 365 nm in the temperature range of 25-100 ^{o}C.

Table S1. ICP analysis of the Pb^{2+}@UiO-66 precursors with different Pb^{2+} concentrations.

Samples	Actual / wt.%
Pb^{2+}@UiO-66-10	10.17
Pb^{2+}@UiO-66-20	15.10
Pb^{2+}@UiO-66-30	18.02
Pb^{2+}@UiO-66-40	20.60
Pb^{2+}@UiO-66-50	22.74
Pb^{2+}@UiO-66-60	25.72

Table S2. ICP analysis of the $MAPbBr_3$@UiO-66 composites.

Samples	Actual / wt.%
$MAPbBr_3$@UiO-66-10	7.69
$MAPbBr_3$@UiO-66-20	11.32
$MAPbBr_3$@UiO-66-30	15.54
$MAPbBr_3$@UiO-66-40	17.27
$MAPbBr_3$@UiO-66-50	19.78
$MAPbBr_3$@UiO-66-60	21.07

Table S3. A summary of PLQYs for the PeQDs@MOF composites.

PeQDs@MOFs composites	PLQY (%)	Ref.
$MAPbBr_3$@MA-$Mn(HCOO)_3$	2.6	[2]
$MAPbBr_3$@Bio-MOF-1	16	[3]
$CsPbBr_{1.2}I_{1.8}$@UiO-67	29.7	[4]
$MAPbBr_3$@MOF-5	37.5	[5]
$CsPbBr_3$@UiO-67	38.5	[4]
$MAPbBr_3$@Pb-MOF	39.6	[6]
$MAPbBr_3$@Eu-BTC	40.2	[7]
$MAPbBr_3$@UiO-66-50	43.3	This work
$MAPbBr_3$@ZJU-28	51.1	[8]
$CsPbBr_3$@MOF-5	52	[9]
$CsPbBr_{0.6}I_{2.4}$@MOF-5	56	[9]
$CsPbBr_3$@ZJU-28	62	[10]

References

1. A. Schaate, P. Roy, A. Godt, J. Lippke, F. Waltz, M. Wiebcke and P. Behrens, *Chem.-Eur. J.*, 2011, **17**, 6643-6651.
2. D. Rambabu, S. Bhattacharyya, T. Singh, M. L. Chakravarthy and T. K. Maji, *Inorg. Chem.*, 2020, **59**, 1436-1443.
3. Q. Zhang, H. Wu, W. Lin, J. Wang and Y. Chi, *J. Solid State Chem.*, 2019, **272**, 221-226.
4. D. Zhang, J. Zhao, Q. Liu and Z. Xia, *Inorg. Chem.*, 2019, **58**, 1690-1696.
5. D. Zhang, Y. Xu, Q. Liu and Z. Xia, *Inorg. Chem.*, 2018, **57**, 4613-4619.
6. C. Zhang, B. Wang, W. Li, S. Huang, L. Kong, Z. Li and L. Li, *Nat. Commun.*, 2017, **8**, 1138.
7. D. Zhang, W. Zhou, Q. Liu and Z. Xia, *ACS Appl. Mater. Interfaces*, 2018, **10**, 27875-27884.
8. H. He, Y. Cui, B. Li, B. Wang, C. Jin, J. Yu, L. Yao, Y. Yang, B. Chen and G. Qian, *Adv. Mater.*, 2019, **31**, 1806897.
9. J. Ren, T. Li, X. Zhou, X. Dong, A. V. Shorokhov, M. B. Semenov, V. D. Krevchik and Y. Wang, *Chem. Eng. J.*, 2019, **358**, 30-39.
10. J. Ren, X. Zhou and Y. Wang, *Chem. Eng. J.*, 2020, **391**, 123622.